Low Temperature Physics/Fizika Nizkikh Temperatur, 2018, v. 44, No. 4, pp. 379–388

Nonlinear dynamics of a two-dimensional Wigner solid on superfluid helium

Yu.P. Monarkha

B. Verkin Institute for Low Temperature Physics and Engineering of the National Academy of Sciences of Ukraine
47 Nauky Ave., Kharkiv 61103, Ukraine
E-mail: monarkha@ilt.kharkov.ua

Received August 16, 2017, published online February 26, 2018

Nonlinear dynamics and transport properties of a 2D Wigner solid (WS) on the free surface of superfluid helium are theoretically studied. The analysis is nonperturbative in the amplitude of the WS velocity. An anomalous nonlinear response of the liquid helium surface to the oscillating motion of the WS is shown to appear when the driving frequency is close to subharmonics of the frequency of a capillary wave (ripplon) whose wave vector coincides with a reciprocal-lattice vector. As a result, the effective mass of surface dimples formed under electrons and the kinetic friction acquire sharp anomalies in the low-frequency range, which affects the mobility and magnetoconductivity of the WS. The results obtained here explain a variety of experimental observations reported previously.

PACS: 73.20.Qt Electron solids;
73.40.–c Electronic transport in interface structures;
67.90.+z Other topics in quantum fluids and solids;
71.45.Lr Charge-density-wave systems.

Keywords: Wigner solid, 2D electron systems, nonlinear transport, superfluid helium.

1. Introduction

A two-dimensional (2D) electron gas bound to the free surface of liquid helium is known to exhibit a phase transition into the Wigner solid (WS) state [1]. In this state, surface electrons are localized in sites of a triangular lattice. The WS of surface electrons is hovering above the liquid surface at the average height of about 100 Å. The surface of liquid helium has no pining centers, therefore, the WS can move along the interface in an ac driving electric field interacting with surface excitations of liquid helium. Electrons forming the Wigner crystal put periodic pressure on the surface of liquid helium, and, therefore, a lattice of surface dimples is formed under electrons [2]. This periodic pressure and the dimple lattice are essential for understanding the linear dynamics of the WS in an ac driving field [3] and for the description of the experiment [1]. An important consequence of the theory is that an oscillating motion of the WS along the surface resonantly excites capillary waves (ripplons) if the driving field frequency ω is close to the frequency of ripplons $\omega_{r,q} = \sqrt{\alpha/\rho q}^{3/2}$ with the wave vector q equal to the electron reciprocal lattice vector $\mathbf{g}$ (here α and ρ are, respectively, the surface tension and mass density of liquid helium).

Since the discovery of Grimes and Adams [1], a number of remarkable nonlinear effects was observed when studying the WS transport along the surface of superfluid ^{4}He. A nonequilibrium melting of the 2D WS indicated by a sharp change in the magnetoresistance of the electron system was reported in Ref. 4. A puzzling nonlinear dependence of the WS magnetoconductivity σ_{xx} ending by a dynamic transition was observed [5,6]. This transition was interpreted as the WS sliding over the sublattice of surface dimples. In the region of small values of the input voltage $V_{\rm in}$, the inverse magnetoconductivity σ_{xx}^{-1} rises rapidly with $V_{\rm in}$ up to its maximum value. Then, in the region of intermediate values of the input voltage, σ_{xx}^{-1} decreases approximately as $1/V_{\rm in}$. A similar region of σ_{xx} proportional to $V_{\rm in}$ observed [7] was explained by an assumption that the Hall velocity of electrons cE/B is limited by the phase velocity of ripplons with the wave vector equal to the electron reciprocal lattice vector $\mathbf{g}$. It was suggested that in this region the electric field E is independent of $V_{\rm in}$, while $\sigma_{xx} \propto V_{\rm in}$. It should be noted also that in that work, the region of low excitation voltage where σ_{xx}^{-1} rises (σ_{xx} decreases) as well as the linear conductivity regime were not detected.

In the absence of a magnetic field, the nonlinear WS mobility was studied in Ref. 8. In this experiment, an initial mobility of the WS is rather high, and it strongly decreases with the amplitude of the driving electric field. This is contrary to the magnetoconductivity data of Refs. 5,6 which indicate that at a smallest $V_{\rm in}$ mobility of the WS is low (though there are no pinning centers above superfluid ^{4}He) and it initially increases with the input voltage. This seeming contradiction should be explained in a strict theory.

Interesting results were obtained in experimental studies [8] of coupled phonon-ripplon modes of the WS on liquid helium in high driving electric fields. At a low excitation voltage the response amplitude as a function of the frequency of the excitation signal shows two maxima whose positions agree with the frequencies of a coupled phonon-ripplon mode [3] calculated for two smallest wave vectors k_1 and k_2 defined by the geometry of the experimental cell. It seems strange that with an increase of the amplitude of the excitation signal positions of these two resonances were observed to shift in opposite (!) directions. Moreover, new low-frequency electron-ripplon resonances were observed away from frequencies of conventional phonon-ripplon coupled modes [3]. These experimental data also require a theoretical explanation (a brief report explaining these effects is given in Ref. 9).

It should be emphasized that contrary to the case of superfluid ^{4}He, the linear regime of the WS transport over the free surface of normal and superfluid ^{3}He was detected [10], and anomalies of WS mobility data were well described by the theory [11]. Moreover, there is a good understanding [12] of the nonlinear WS mobility on the surface of liquid ^{3}He. In this case, a good theoretical description is possible owing to strong damping effects in the Fermi liquid which limit the mobility of surface dimples. We conclude that remarkable nonlinear phenomena reported for the WS transport over superfluid ^{4}He are induced by the extremely small damping of ripplons. According to the quantum hydrodynamical model [13], the damping of capillary waves

$$\gamma_q = \frac{\pi^2}{60}\frac{\hbar}{\rho}\left(\frac{T}{\hbar \mathrm{v}_1}\right)^4 q \qquad (1)$$

decreases fast with lowering temperature. Here v_1 is the first sound velocity, and q is a wave vector. For typical experimental conditions (electron density $n_e = 6\cdot 10^8\,\mathrm{cm}^{-2}$ and $0.4\ \mathrm{K} \geq T \geq 0.1\ \mathrm{K}$), the ratio $\gamma_g/\omega_{r,g}$ varies from 10^{-4} to 10^{-7} even for the smallest reciprocal-lattice vector $g = g_1$.

In this work, we report a theoretical investigation of nonlinear dynamics and nonlinear transport properties of the 2D WS over superfluid helium caused by extremely small damping of capillary waves. Considering the regime of a given current, we found an exact expression for the medium response force acting on the dimple sublattice which consists of two parts representing the kinetic friction and dimple inertia. It is remarkable that the effective mass of surface dimples and the effective collision frequency of the kinetic friction change sharply in the vicinity of subharmonic frequencies of ripplons $\omega_{r,g}/m$ (here $m = 2, 3, ...$), which affects the nonlinear transport of the WS and phonon-ripplon coupling. In the presence of a magnetic field directed normally to the surface, the nonlinear magnetoconductivity expression obtained is not reduced to a simple Drude form which explains differences between mobility and magnetoconductivity data reported previously. At sufficiently strong driving fields, the nonlinear magnetoconductivity σ_{xx} obtained here becomes negative, which causes instability and WS melting. This effect can be considered as an alternative explanation of dynamic transitions observed in the experiments [4–6].

2. Model description

The localization of an electron in a lattice site is accompanied by a displacement of the liquid helium surface $\xi(\mathbf{r})$ from the equilibrium flat shape caused by the electron pressure. This deformation of the gas-liquid interface called the dimple lattice is the main origin of nonlinear effects in the WS transport. Under usual conditions, the dimple lattice does not change the melting temperature of the WS, but it strongly affects its dynamics, especially in the low frequency range. In terms of electron displacements $\mathbf{s}_l$ from a lattice site $\mathbf{R}_l$, the WS coupling with capillary waves is described by the interaction Hamiltonian

$$H_{\rm int} = \sum_{\mathbf{q}} U_q \xi_{\mathbf{q}} \sum_{\mathbf{l}} \exp\left[i\mathbf{q}(\mathbf{R}_l + \mathbf{s}_l)\right], \qquad (2)$$

where $\xi_{\mathbf{q}}$ is the Fourier transforms of the surface displacement, U_q is the coupling function for the electron-ripplon interaction [14] (in the limit of strong holding fields $E_\perp$, it equals $eE_\perp$). Displacements $\mathbf{s}_l$ consist of a high-frequency part $\mathbf{s}_{\mathrm{f},l}$, caused by thermal vibrations, and a low-frequency part $\mathbf{s}_{\mathrm{s},l}$ due to slow WS motion in a driving electric field. In this work, the low-frequency part is assumed to be uniform $\mathbf{s}_{\mathrm{s},l} \equiv \mathbf{s}(t)$.

Taking into account an expression for the Hamiltonian of free ripplons [14] and Eq. (2), the equation for $\xi_{\mathbf{q}}$ can be found in the following form

$$\ddot{\xi}_{\mathbf{g}} + 2\gamma_g \dot{\xi}_{\mathbf{g}} + \omega_{r,g}^2 \xi_{\mathbf{g}} = -\frac{\tilde{U}_g n_e g}{\rho} \mathrm{e}^{-i\mathbf{g}\cdot\mathbf{s}(t)}, \qquad (3)$$

where $\tilde{U}_q = U_q \exp\left(-q^2\left\langle s_{\mathrm{f}}^2\right\rangle/4\right)$, a Debye-Waller factor appears due to averaging over fast (high-frequency) modes, $\left\langle s_{\mathrm{f}}^2\right\rangle$ is the contribution to the mean-square displacement from fast modes, and γ_g describes ripplon damping. The right side of Eq. (3) represents the periodic electron pressure acting on the free surface of liquid helium. If $\mathbf{s}(t) = 0$, the first two terms of Eq. (3) are zero and the rest terms yield the shape of a motionless dimple lattice.

In the conventional theory of the WS coupling with ripplons [3], the exponential function entering the right side of Eq. (3) is expanded up to a linear (in $\mathbf{g}\cdot\mathbf{s}$) term. This term, representing the first harmonic of ω in the electron pressure, is responsible for a resonant increase of the ripplon field $\xi_{\mathbf{g}}$ when $\omega \to \omega_{r,g}$. In a nonlinear theory, the electron pressure contains superharmonics of ω due to higher expansion terms. Thus, the right side of Eq. (3) contains terms proportional to $\exp(-im\omega t)$ [here we assume that $\mathbf{s}(t) \propto \exp(-i\omega t)$ and $m = 2, 3,...$]. These superharmonic terms of the electron pressure lead to a resonant increase of $\xi_{\mathbf{g}}$ if $m\omega \to \omega_{r,g}$. In other words, we expect a resonant increase of the medium response (the dimple effective mass and kinetic friction) if the WS is driven at a frequency which is close to a subharmonic of typical ripplon frequencies: $\omega \to \omega_{r,g}/m$. In the following, we will not expand the right side of Eq. (3) assuming that the parameter $\mathbf{g}\cdot\mathbf{s}$ can be large.

As noted in the Introduction, at low temperatures the ripplon damping of pure ^{4}He is extremely small according to Eq. (1). In the presence of impurity ^{3}He atoms (dilute ^{3}He–^{4}He solutions), the ripplon damping is substantially increased. For the viscous regime, one can find

$$\gamma_q = \frac{\eta}{\rho} q^2 \phi\left(\omega\rho/\eta q^2\right), \phi(x) = 2 - \frac{\sqrt{2}}{x}\left(\sqrt{1+x^2}-1\right)^{1/2}, \quad (4)$$

where η is the viscosity of the solution. In this case, our model should be improved by an additional frequency dependent term $-\delta_g^2(\omega)\xi_g$ in the left side of Eq. (3), where $\delta_g^2(\omega) = \omega^2\zeta(\omega\rho/\eta g^2)$ and

$$\zeta(x) = \frac{4}{x^2}\left[\frac{1}{\sqrt{2}}\left(\sqrt{1+x^2}+1\right)^{1/2} - 1\right]. \quad (5)$$

In the limit $\omega\rho/\eta g^2 \ll 1$, we have $\delta_g^2(\omega) \to \omega^2/2$ which just increases inertia of the dimple lattice and changes parameters of Eq. (3) by the numerical factor $2/3$.

At low temperatures, impurity quasiparticles enter the long mean-free-path regime, and the ripplon damping is caused by their reflection from an uneven surface. According to Ref. 15, for specular reflection, we have

$$\gamma_q^{(s)} = \frac{\kappa(T)}{2\rho} q, \quad \kappa(T) = \kappa(0) 2\left(\frac{T}{T_F}\right)^2 F\left(e^{\mu(\mathrm{qp})}/T\right), \quad (6)$$

where

$$\kappa(0) = \frac{p_F^4}{4\pi^2\hbar^3}, \quad F(z) = z\int_0^\infty \frac{x}{e^x + z}dx, \quad (7)$$

T_F and p_F are, respectively, the Fermi temperature and the Fermi momentum of impurity atoms. The ripplon damping defined by Eq. (6) has the same dependence on q as that obtained for pure ^{4}He, still it has different dependence on temperature: $\gamma_q \to$ const if $T \to 0$. Assuming that a fraction of incoming quasiparticles r_a can be reflected diffusively from the the surface layer of ^{3}He atoms which is not involved in the horizontal motion of the dimple lattice [15], we have $\gamma_q = (1-3r_a/4)\gamma_q^{(s)}$. For impurity concentration $c_3 = 6.1\%$ and electron density $n_e = 1.4\cdot 10^8$ cm^{-2}, the ratio $\gamma_g/\omega_{r,g}$ can be increased up to about 0.4. Thus, any reasonably small ratio $\gamma_g/\omega_{r,g}$ can be realized in an experiment with the WS on the surface of ^{3}He–^{4}He mixtures.

A solution $\xi_g(t)$ of the model equation (3) can be found trivially in an integral form [17], and the force acting on the WS by surface dimples, defined as $\mathbf{F}_D = -\left\langle \sum_e \partial H_{\mathrm{int}}/\partial \mathbf{r}_e \right\rangle_f$ (here $\langle ... \rangle_f$ denotes averaging over fast modes), can be represented as

$$\frac{\mathbf{F}_D}{N_e} = -\sum_{\mathbf{g}} \mathbf{g} \frac{n_e g \tilde{U}_g^2}{\rho\hat{\omega}_g^2} \mathcal{F}_{\mathbf{g}}(t), \quad (8)$$

where

$$\mathcal{F}_{\mathbf{g}}(t) = \hat{\omega}_g \int_0^\infty \sin(\hat{\omega}_g\tau) e^{-\gamma_g\tau} \sin\left\{\mathbf{g}\cdot\left[\mathbf{s}(t) - \mathbf{s}(t-\tau)\right]\right\} d\tau, \quad (9)$$

and $\hat{\omega}_g = \sqrt{\omega_{r,g}^2 - \gamma_g^2}$. Equations (8) and (9) determine the nonlinear response of the liquid helium surface to an oscillating motion of the WS.

The equation of motion for an electron displacement $\mathbf{s}(t)$ including the medium response force $\mathbf{F}_D(t)$ represents a complicated nonlinear equation which is very difficult to solve for a given driving electric field $\mathbf{E}(t)$. Remarkably, an inverse problem of finding $\mathbf{E}(t)$ for a given current can be solved exactly. It should be noted that, in experiments on WS transport, the driving electric field is often adjusted to the current owing to electron redistribution which screens external potential variations. Therefore, the regime of a given current is realized at least partly. This conclusion is supported by experimental observations [12,16] of regions with $dE/du < 0$, where u is the WS velocity.

In the absence of a magnetic field, we shall consider a simple periodic dependence $\mathbf{s}(t) = \mathbf{s}_0 \sin(\omega t)$ and assume that the x-axis is directed along $\mathbf{s}_0$. Then, the periodic function $F_D^{(x)}(t)$ can be represented as a Fourier series

$$\frac{F_D^{(x)}}{N_e} = -m_e \sum_{k=1}^\infty \left[\nu_k \omega s_0 \cos(k\omega t) - \chi_k \omega^2 s_0 \sin(k\omega t)\right], \quad (10)$$

where ν_k and χ_k are two kinds of Fourier coefficients defined by the well known rule. The factors $m_e\omega s_0$ and $m_e\omega^2 s_0$ (here m_e is the free electron mass) are introduced in order to make proper dimensions for ν_k and χ_k. We shall see that ν_1 is an effective collision frequency due to kinetic friction of surface dimples, while χ_1 is the ratio of the dimple effective mass m_D to the free electron mass ($\chi_1 = m_D/m_e$).

According to Eq. (10), the force acting on the WS contains the first and higher harmonics of ω. Since the other terms of the equation of motion for an electron displacement $\mathbf{s}(t)$ are linear, only the first harmonics of $F_D^{(x)}(t)$ are important for obtaining the WS conductivity and the secular equation for coupled phonon-ripplon modes. Therefore, we can ignore the higher harmonics of ω in Eq. (10) (though there is no problem with calculation of ν_k and χ_k for an arbitrary k), and omit the subscript 1 assuming $\nu_1 \equiv \nu_D$ and $\chi_1 = \chi$. Direct calculations yield

$$\nu_D = \sum_{\mathbf{g}} g_x^2 \frac{n_e g \tilde{U}_g^2}{m_e \rho \hat{\omega}_g^3} \mathcal{N}\left(g_x s_0, \frac{\omega}{\hat{\omega}_g}, \frac{\gamma_g}{\hat{\omega}_g} \right), \tag{11}$$

$$\chi = \sum_{\mathbf{g}} g_x^2 \frac{n_e g \tilde{U}_g^2}{m_e \rho \hat{\omega}_g^4} \mathcal{M}\left(g_x s_0, \frac{\omega}{\hat{\omega}_g}, \frac{\gamma_g}{\hat{\omega}_g} \right), \tag{12}$$

where we introduced the following functions

$$\mathcal{N}(a,\omega',\gamma') = \frac{1}{\omega' a} Q_\nu(a,\omega',\gamma'), \tag{13}$$

$$Q_\nu(a,\omega',\gamma') = 2\int_0^\infty \sin(x) e^{-\gamma' x} \cos\left(\frac{\omega' x}{2}\right) J_1\left(2a \sin\left(\frac{\omega' x}{2}\right)\right) dx, \tag{14}$$

$$\mathcal{M}(a,\omega',\gamma') = -\frac{1}{(\omega')^2 a} Q_M(a,\omega',\gamma'), \tag{15}$$

$$Q_M(a,\omega',\gamma') = 2\int_0^\infty \sin(x) e^{-\gamma' x} \sin\left(\frac{\omega' x}{2}\right) J_1\left(2a \sin\left(\frac{\omega' x}{2}\right)\right) dx, \tag{16}$$

and $J_1(z)$ is the Bessel function. Properties of the function $Q_\nu(a,\omega',\gamma')$ were partly investigated in the low-frequency limit [17] where a broadening of the Bragg-Cherenkov threshold occurred. Still, the nonlinear WS mobility and conductivity were not investigated because the dimple mass-function $\mathcal{M}(a,\omega',\gamma')$ was not studied, and superharmonic resonances of the ripplon field at $m\omega \to \omega_{r,g}$ were not disclosed.

It should be noted that even first harmonics of $F_D^{(x)}(t)$ in Eq. (10) defined by ν_D and χ (or equivalently, by Q_ν and Q_M) contain contributions from higher harmonics of the electron pressure entering the right side of Eq. (3). This can be seen from dependencies of $\mathcal{N}(a,\omega',\gamma')$ and $\mathcal{M}(a,\omega',\gamma')$ on the dimensionless frequency $\omega' = \omega/\hat{\omega}_g$ calculated for different values of the nonlinear parameter $a = g_x s_0$. Fig. 1 indicates that $\mathcal{N}(a,\omega',\gamma')$ has sharp maxima at $\omega' = 1/m$ ($\omega = \hat{\omega}_g/m$) whose intensities depend on a in a non-monotonic way. As the parameter a increases, the distribution of maxima shifts strongly into the low-frequency range.

The function $\mathcal{M}(a,\omega',\gamma')$ shown in Fig. 2 sharply changes its sign near points $\omega' = 1/m$. In the limiting case

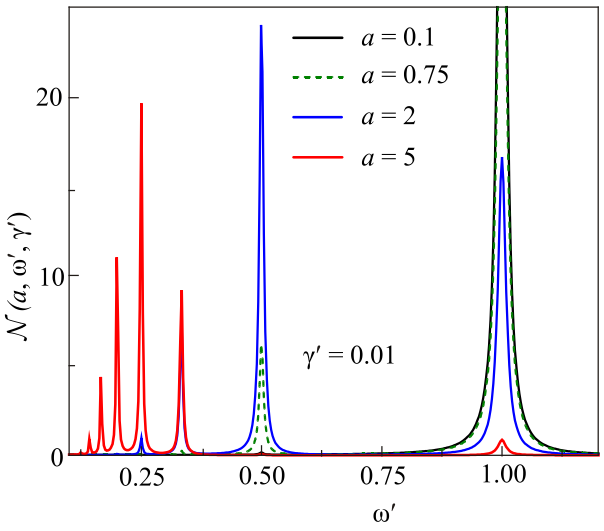

Fig. 1. (Color online) The dimensionless collision frequency function $\mathcal{N}(a,\omega',\gamma')$ vs. $\omega' = \omega/\hat{\omega}_{r,g}$ calculated for four values of the parameter $a = g_x s_0$.

$\gamma' = \gamma_g/\hat{\omega}_g \to 0$, the frequency dependence of $\mathcal{M}(a,\omega',0)$ can be fitted by a simple function [9]

$$\mathcal{M}(a,\omega',0) = \sum_{m=1}^{\infty} \frac{S_m}{1/m^2 - (\omega')^2}, \tag{17}$$

where the weight of a singularity S_m is a non-monotonic function of a. In the linear regime, only the first term in the sum is important: $S_1 = 1$, and $S_m = 0$ if $m > 1$. With an increase of the nonlinear parameter a, the distribution of S_m is shifted in the range of large m. It should be noted that a strong increase of a reduces S_1 and changes its sign.

Thus, in the nonlinear regime, the both functions $\mathcal{N}(a,\omega',\gamma')$ and $\mathcal{M}(a,\omega',\gamma')$ are affected strongly by

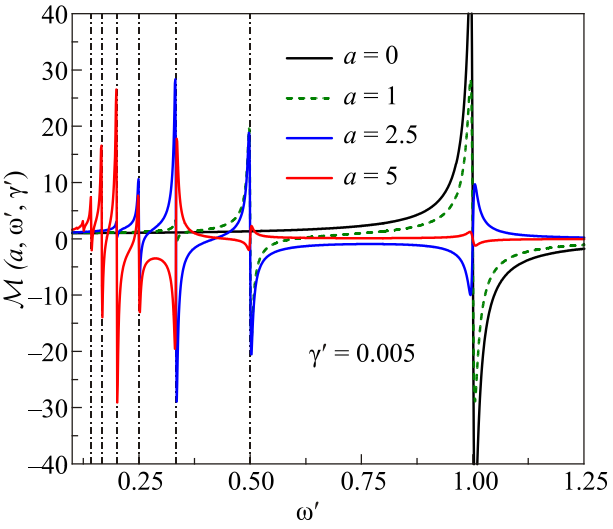

Fig. 2. (Color online) The dimensionless dimple-mass function $\mathcal{M}(a,\omega',\gamma')$ vs. $\omega' = \omega/\hat{\omega}_{r,g}$ calculated for four values of the parameter $a = g_x s_0$.

superharmonic resonances of the ripplon field. The effective collision frequency ν_D and the dimple effective mass $m_D = \chi m_e$ change sharply when the WS is driven by a frequency ω which is close to subharmonics of the typical ripplon frequencies $\omega = \omega_{r,g} / m$.

The amplitude of the WS velocity $u_0 = \omega s_0$. Therefore, the nonlinear parameter $a = g_x s_0$ can be represented as $a = u'/\omega'$, where $u' = u_0 / u_{g,x}$ and $u_{g,x} = \hat{\omega}_g / g_x$. This allows us to calculate $\mathcal{N}$ and $\mathcal{M}$ as functions of the dimensionless velocity u' near the singular points $\omega' = 1/m$. For example, consider $\omega' = 1/3$ and a close frequency $\omega' = 0.331$. Under these conditions, the function $\mathcal{N}(u'/\omega', \omega', \gamma')$ is shown in Fig. 3 for three values of γ'. It is remarkable that $\mathcal{N}$ is large far below the Bragg-Cherenkov threshold condition ($u' = 1$) where a steady motion of the WS starts emitting ripplons [18]. Moreover, curves calculated for $\omega' = 1/3$ and for the close frequency have different evolutions of their maxima with lowering the damping parameter. The maximum of $\mathcal{N}$ calculated for $\omega' = 1/3$ monotonously increases with decreasing γ' (red dashed and dotted curves), while the maximum calculated for a very close frequency $\omega' = 0.331$ increases only in a short range of γ' (blue dashed curve) and decreases at sufficiently low γ' (blue dotted curve). A similar behavior of $\mathcal{N}$ is disclosed for a frequency slightly larger than $1/3$ and in the vicinity of other singular points $1/m$.

The dimensionless mass function $\mathcal{M}(u'/\omega', \omega', \gamma')$ is shown in Fig. 4 for $\omega' = 1/3$ and two close frequencies. Calculations were performed using three values of the damping parameter γ'. For the singular point $\omega' = 1/3$ (red), the $\mathcal{M}$ as a function of u' is practically independent of the damping parameter. It is remarkable that already very small changes of the driving frequency $\omega' = 0.32$ (blue) and $\omega' = 0.34$ (green) lead to strong (even qualitative) changes in the dependence of $\mathcal{M}$ on the WS velocity

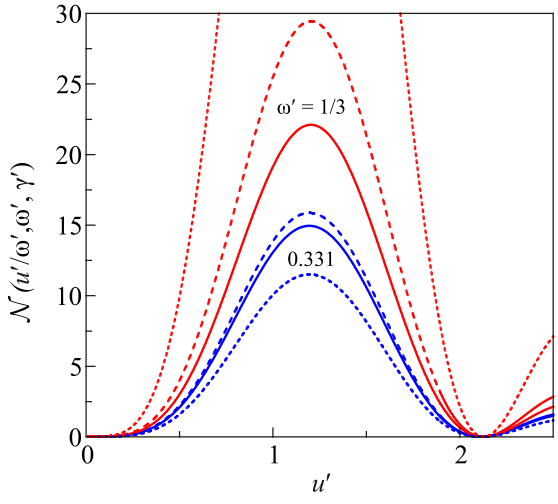

Fig. 3. (Color online) The $\mathcal{N}(u'/\omega', \omega', \gamma')$ vs. dimensionless velocity $u' = u_0 / u_{g,x}$ calculated for $\omega' = 1/3$ (red curves) and $\omega' = 0.331$ (blue curves), and for three values of γ': 0.01 (solid), 0.0075 (dashed), and 0.003 (dotted).

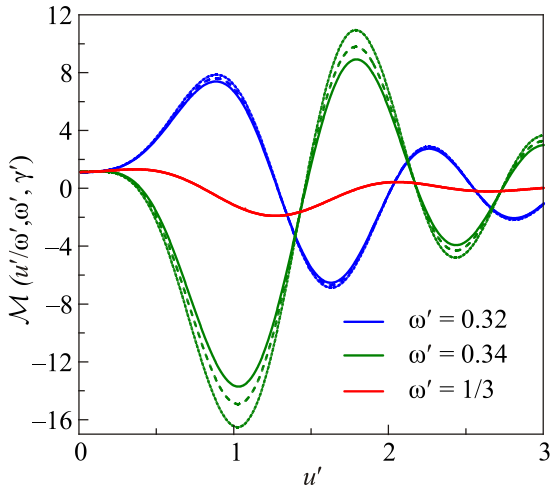

Fig. 4. (Color online) The $\mathcal{M}(u'/\omega', \omega', \gamma')$ vs. dimensionless velocity $u' = u_0 / u_{g,x}$ calculated for three values of ω' and for three values of γ': 0.01 (solid), 0.0075 (dashed), and 0.003 (dotted).

u', and near extrema the results of calculations become dependent on the damping parameter. A similar behavior of $\mathcal{M}$ is found also for $\omega' \to 1/2$ and near lower singular points $1/m$.

The results shown in Figs. 3 and 4 lead to the following important conclusions. In the low frequency range $\omega' \ll 1$, a frequency ω' can be rather close to a singular point $1/m$. Then, a small variation in the electron density n_s affects $\omega' = \omega / \hat{\omega}_g$ and can cause large (even giant) changes in the nonlinear conductivity of the WS, which may lead to a mistaken conclusion that data are not reproducible. In an experiment employing the transmission line model, there are long wave-length density variations along the electron pool. Therefore, according to Fig. 3, the area of the pool which approaches the condition $\omega / \hat{\omega}_g \to 1/m$ has huge friction causing a dynamic "pining" of the WS to the liquid substrate. Of course, this pinning is limited by the wave-length of the density variation. Moreover, as we shall see, in the nonlinear regime, data obtained employing different methods can bring different mobility results.

3. Nonlinear mobility

In the absence of a magnetic field, the WS mobility and conductivity can be found from the force balance equation

$$m_e \dot{u} = -eE(t) + \frac{F_D^{(x)}(t)}{N_e} - m_e \nu_e u \qquad (18)$$

where $u = \omega s_0 \cos(\omega t)$, and ν_e is the electron collision frequency due to scattering with thermally excited ripplons. For the given current $j_x = -en_s \omega s_0 \cos \omega t$, this equation determines the electric field $E(t)$ whose first harmonic (usually measured in an experiment) can be generally written as $E(t) = E_0 \sin(\omega t + \beta)$. The expression for $F_D^{(x)}(t)$ obtained above yields

$$\sin\beta = -\frac{\nu}{\sqrt{\nu^2 + \mathcal{Z}^2\omega^2}} \tag{19}$$

and the relationship between amplitudes

$$\sqrt{(\nu s_0\omega)^2 + \mathcal{Z}^2\omega^4 s_0^2} = \frac{e}{m_e}E_0, \tag{20}$$

where $\mathcal{Z}(\omega, u_0) = 1 + \chi(\omega, u_0)$ represents dimensionless effective mass of an electron bound to a surface dimple, $u_0 = \omega s_0$ and $\nu = \nu_D + \nu_e$.

To obtain the conductivity expression we shall use the change of the time variable $\omega t + \beta = \omega t' + \frac{\pi}{2}$ which transforms the ac electric field into the conventional form $E(t') = E_0\cos(\omega t')$. In this case, using Eqs. (19) and (20) the WS current can be transformed into the usual two-component form

$$j = E_0\cos(\omega t')\mathrm{Re}\sigma + E_0\sin(\omega t')\mathrm{Im}\sigma, \tag{21}$$

where the first component, oscillating in phase with $E(t')$, usually determines the real part of conductivity, while the out-of-phase component determines the quantity which is called the imaginary part of conductivity:

$$\mathrm{Re}\sigma = \frac{e^2 n_e}{m_e}\frac{\nu}{\nu^2 + \mathcal{Z}^2\omega^2},$$

$$\mathrm{Im}\sigma = \frac{e^2 n_e}{m_e}\frac{\mathcal{Z}\omega}{\nu^2 + \mathcal{Z}^2\omega^2}. \tag{22}$$

The WS mobility is defined as $\mu = \mathrm{Re}\sigma / en_e$.

The Eq. (20) allows obtaining the velocity-field characteristic for the amplitudes E_0 and u_0. Contrary to the case of pure ^{3}He, here this characteristic depends also on the effective mass function $\mathcal{Z}(\omega, u_0)$ and ν_e. In order to calculate ν_e, we use a high temperature approximation for the dynamic structure factor of the 2D WS where the average kinetic energy of an electron in the WS state replaces the temperature [19]. For the conditions of the experiment [8], typical $u_0 - E_0$ characteristics are shown in Fig. 5, where $u_R = \omega_{r,g_1}/g_1$. Assuming that our results can be applied (at least qualitatively) to the regime of a given field, we conclude that at a certain threshold value of E_0 the balance of forces is broken and there should be a bistability jump (transition) to a high velocity branch. In the regime of a given current, the region with $\partial u_0 / \partial E_0 < 0$ can be observed.

Using $u_0 - E_0$ characteristics of Fig. 5, the Eq. (22) and the relationship $\mu = \mathrm{Re}\sigma / en_s$, the nonlinear mobility of the WS $\mu(E_0)$ is calculated and shown in Fig. 6 for two values of ω. Before the bistability jump shown by an arrow, the calculated dependence $\mu(E_0)$ is in a qualitative agreement with experimental observation [8]. It should be noted that even a small region with negative $\partial\mu / \partial E_0$ is noticeable in the experimental data set [8]. The figure indicates that the threshold field E_{th} and mobility values of small E_0 depend

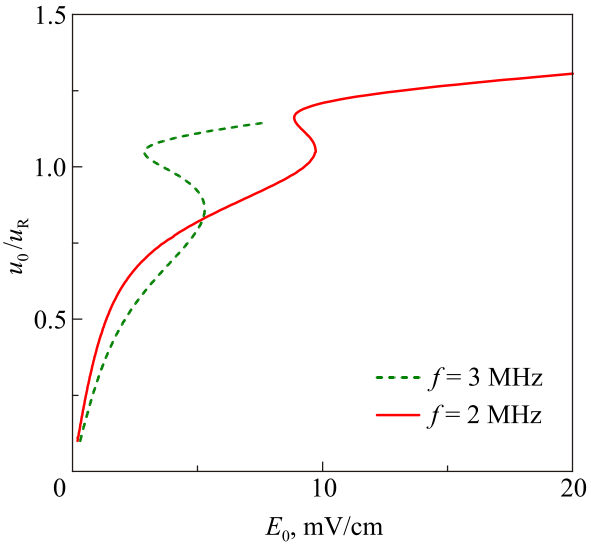

Fig. 5. (Color online) Velocity-field characteristics calculated for two typical frequencies $f = \omega/2\pi = 2$ MHz (solid) and 3 MHz (dashed). The damping parameter $\gamma' = 0.005$. The other conditions are the same as in the experiment [8].

strongly on ω. After the jump, the mobility curve was calculated assuming that the WS state survives the transition to a high velocity branch and ν_e is independent of E_0. Experimental data indicate that after the jump which occurs at $E_0 \approx 10$ mV/cm, the electron mobility steadily increases with E_0 similar to the mobility of a 2D electron gas, and most probably the WS is broken.

The experimental method [20] allows measuring the quantity $m_e\omega\mathcal{Z}/n_e e^2$ which is proportional to the effective mass function $\mathcal{Z}$. Under the experimental conditions [20], theoretical calculations using the expression for $\mathcal{Z}$ obtained here are shown in Fig. 7 for three typical values of ω. As expected, at a fixed electron density ($n_e = 12.6\cdot10^8\,\mathrm{cm}^{-2}$) the peculiarity of the function $\mathcal{Z}(E_0)$

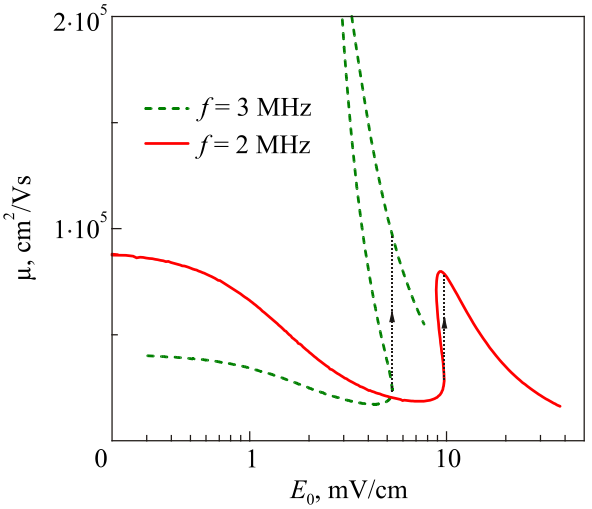

Fig. 6. (Color online) Mobility of the WS vs the amplitude of the driving electric field. Conditions are the same as in Fig. 5.

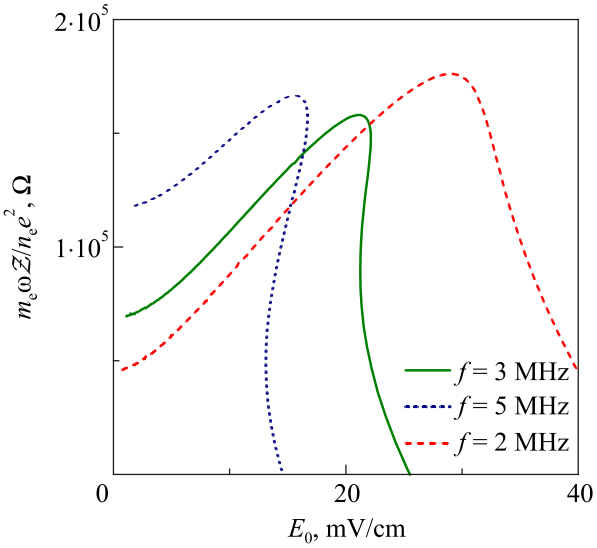

Fig. 7. (Color online) The quantity $m_e\omega\mathcal{Z}/n_e e^2$ vs. the amplitude of the driving electric field calculated for three frequencies of $E(t)$. Other conditions are the same as in the experiment [20].

strongly depends on the driving frequency ω. For example, the bistability range, which is prominent at $f = \omega/2\pi = 5$ MHz (dotted) and noticeable at $f = 3$ MHz (solid), disappears already at $f = 2$ MHz (dashed). The observed [20] shape of $m_e\omega\mathcal{Z}/n_e e^2$ is in agreement with the solid curve of Fig. 7. The position of the maxima is about 2.3 times higher than the value of the linear regime which also agrees with experimental observations.

4. Excitation of coupled phonon-ripplon modes

If longitudinal phonons of the WS with a wavevector k defined by the geometry of the cell can be exited in an experiment, the equation of motion for electron displacements acquires an additional restoring force. Considering only a long wave-length excitation ($k \ll g_1$), the conductivity of the WS can be represented as

$$\mathrm{Re}\sigma(k) = \frac{e^2 n_e \nu}{m_e\left\{\nu^2 + \left[\mathcal{Z} - \Omega_l^2(k)/\omega^2\right]^2 \omega^2\right\}}, \qquad (23)$$

where $\Omega_l(k)$ is the spectrum of longitudinal phonons of the WS. Here the nonlinear effect is included in definitions of ν_D ($\nu = \nu_D + \nu_e$) and $\mathcal{Z}$. In the nonlinear regime, the effective mass function $\mathcal{Z}$ has new singular points near $\omega = \omega_{r,g}/m$, and, therefore, one can expect new resonances of $\mathrm{Re}\sigma(k)$ when

$$\mathcal{Z} - \Omega_l^2(k)/\omega^2 = 0. \qquad (24)$$

The Eq. (24) is a secular equation for coupled phonon-ripplon modes. Solutions of this equation were analyzed in Ref. 9. Here we investigate the frequency dependence of $\mathrm{Re}\sigma$ proportional to the energy absorbtion in a nonlinear regime.

The spectrum of $\mathrm{Re}\sigma(k,\omega)$ is shown in Fig. 8 for different values of the nonlinear parameter $a_1 = g_1 s_0$ and for two nearest wavevectors k_1 and k_2 corresponding to the conditions of the experiment [8]. At a low excitation level ($a_1 = 0.1$) we have two pronounced maxima corresponding to conventional phonon-ripplon coupled modes. At a higher excitation level ($a_1 = 0.5$) these maxima are shifted in opposite (!) directions because they were initially placed at the opposite sides of the singular point $\omega/\omega_1 = 1/2$ ($\omega_1 = \omega_{r,g_1}$) where $\mathcal{M}(\omega')$ rapidly changes as an odd function (see Fig. 2). For even higher excitation levels ($a_1 = 1$ and $a_1 = 2$), new low-frequency resonances appear due to phonon-ripplon coupling near subharmonics of $\omega_{r,g}$. It should be noted that in a real experiment the inhomogeneous broadening could affect the new resonances especially for $k = k_2$. Anyway, the theoretical results presented in Fig. 8 explain why the positions of conventional phonon-ripplon resonances corresponding to k_1 and k_2 shift in opposite directions with an increase of the excitation power. The appearance of new low-frequency resonances is also in agreement with experimental observations [8].

5. Nonlinear magnetoconductivity

Magnetoconductivity of the WS usually is measured under the condition that the Hall velocity is much higher than the drift velocity along the direction of the electric field (here the x-axis is fixed to be parallel to the electric field). In the presence of a strong magnetic field B directed perpendicular to the surface, assuming $s_y = s_{y,s}\sin(\omega t)$, we have to consider $s_x = s_{x,s}\sin(\omega t) + s_{x,c}\cos(\omega t)$ to satisfy equations of motion for electron displacements.

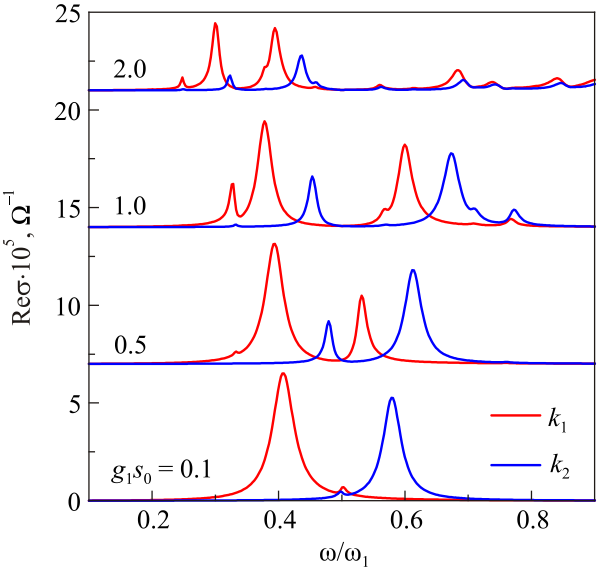

Fig. 8. (Color online) Frequency dependence of $\mathrm{Re}\sigma(\omega,k)$ calculated for two lowest wavevectors k_1 (red curves) and k_2 (blue curves). For the sake of clarity, each curve of a higher excitation level is shifted up by $7\cdot10^{-5}\,\Omega^{-1}$ with respect to the zero level of the previous curve. The damping parameter $\gamma' = 0.01$.

The amplitude of the Hall motion $s_{y,s}$ is much larger than $s_{x,s}$ and $s_{x,c}$. Contrary to the mobility calculations given above, now we should describe two components of the force acting on the WS by surface dimples: $F_D^{(x)}$ and $F_D^{(y)}$. According to Eqs. (8) and (9), $F_D^{(x)}$ and $F_D^{(y)}$ contain factors g_x and g_y, respectively, and, therefore, the function $\mathcal{F}_{\mathbf{g}}(t)$ should be treated differently when expanding it in small $g_x s_x$. We shall use superscripts (x) and (y) to distinguish these two cases. Considering the y component of the force, we can neglect s_x as compared to s_y and use the following approximation $\mathcal{F}_{\mathbf{g}}(t) \simeq \mathcal{F}_{\mathbf{g}}^{(y)}(t)$ with

$$\mathcal{F}_{\mathbf{g}}^{(y)} = \hat{\omega}_g \int_0^\infty \sin(\hat{\omega}_g \tau) e^{-\gamma_g \tau} \sin\left\{ g_y \left[s_y(t) - s_y(t-\tau) \right] \right\} d\tau, \tag{25}$$

because the integral is an odd function of g_y.

The Eq. (25) can be calculated in the way similar to that described above. For major terms of the Fourier series, we have

$$\frac{F_{\mathrm{D}}^{(y)}}{N_e} = -m_e \left[\nu_y \omega s_{\mathrm{s},y} \cos(\omega t) - \chi_y \omega^2 s_{\mathrm{s},y} \sin(\omega t) \right], \tag{26}$$

where

$$\nu_p = \sum_{\mathbf{g}} g_p^2 \frac{n_e g \tilde{U}_g^2}{m_e \rho \hat{\omega}_g^3} \mathcal{N}(g_y s_{\mathrm{s},y}, \omega/\hat{\omega}_g, \gamma_g/\hat{\omega}_g), \tag{27}$$

$$\chi_p = \sum_{\mathbf{g}} g_p^2 \frac{n_e g \tilde{U}_g^2}{m_e \rho \hat{\omega}_g^4} \mathcal{M}(g_y s_{\mathrm{s},y}, \omega/\hat{\omega}_g, \gamma_g/\hat{\omega}_g), \tag{28}$$

and $p = x, y$ is a subscript. As compared to the mobility treatment, here we have a different parameter $a = g_y s_{\mathrm{s},y}$ describing an excitation level.

Considering the $F_D^{(x)}$ component, one cannot use the approximation of Eq. (25) because the integral is an even function of g_x, and this approximation yields $F_D^{(x)} = 0$. Therefore, in this case, $\mathcal{F}_{\mathbf{g}}(t)$ should be expanded up to linear terms of $g_x s_x$:

$$\mathcal{F}_{\mathbf{g}}^{(x)} \simeq \hat{\omega}_g \int_0^\infty \sin(\hat{\omega}_g \tau) e^{-\gamma_g \tau} g_x \left[s_x(t) - s_x(t-\tau) \right] \times$$

$$\times \cos\left\{ g_y \left[s_y(t) - s_y(t-\tau) \right] \right\} d\tau. \tag{29}$$

Here the term independent of $g_x s_x$ [similar to that of Eq. (25)] is neglected because it gives zero result after summation over all $\mathbf{g}$. Formally, we can represent $\mathcal{F}_{\mathbf{g}}(t) \simeq \mathcal{F}_{\mathbf{g}}^{(y)}(t) + \mathcal{F}_{\mathbf{g}}^{(x)}(t)$, where the first term is important only for $F_D^{(y)}$ while the second term is important only for $F_D^{(x)}$.

Inserting $s_x = s_{s,x} \sin(\omega t) + s_{c,x} \cos(\omega t)$ and $s_y = s_{y,s} \sin(\omega t)$ into Eq. (29) gives two different terms. The term proportional $s_{s,x}$ can be represented as a derivative with respect to a, while the term proportional to $s_{c,x}$ can be represented as a time derivative. For the chosen dependence $s_x(t)$, the WS velocity component along the x-axis is a sum $u_x(t) + u_x'(t)$, where $u_x(t) = -\omega s_{x,c} \sin(\omega t)$ and $u_x'(t) = \omega s_{x,s} \cos(\omega t)$ (here and below the stroke means that a quantity originates from the sin-term of s_x). An analysis of the Fourier coefficients indicates that now $F_D^{(x)}$ contains additional friction and inertia components

$$\frac{F_D^{(x)}}{N_e} = -m_e \left[\nu_x u_x + \nu_x' u_x' + \chi_x \dot{u}_x + \chi_x' \dot{u}_x' \right] \tag{30}$$

where ν_x and χ_x are described by Eqs.(27) and (28)),

$$\nu_x' = \sum_{\mathbf{g}} g_x^2 \frac{n_e g \tilde{U}_g^2}{m_e \rho \hat{\omega}_g^3} \mathcal{N}_d \left(g_y s_{y,s}, \frac{\omega}{\hat{\omega}_g}, \frac{\gamma_g}{\hat{\omega}_g} \right), \tag{31}$$

$$\chi_x' = \sum_{\mathbf{g}} g_x^2 \frac{n_e g \tilde{U}_g^2}{m_e \rho \hat{\omega}_g^4} \mathcal{M}_d \left(g_y s_{y,s}, \frac{\omega}{\hat{\omega}_g}, \frac{\gamma_g}{\hat{\omega}_g} \right), \tag{32}$$

and

$$\mathcal{N}_d(a, \omega, \gamma) = \frac{1}{\omega} \frac{\partial}{\partial a} Q_\nu(a, \omega, \gamma), \tag{33}$$

$$\mathcal{M}_d(a, \omega, \gamma) = -\frac{1}{\omega^2} \frac{\partial}{\partial a} Q_M(a, \omega, \gamma). \tag{34}$$

It should be noted that $\mathcal{N}_d(a, \omega, \gamma)$ contains a derivative $\partial Q_\nu(a, \omega, \gamma)/\partial a$ which at a certain condition can become negative causing instability and melting of the WS.

In order to proceed with conductivity calculations, we have to introduce new dimensionless inertia functions $\mathcal{Z}_p = 1 + \chi_p$ and $\mathcal{Z}_x' = 1 + \chi_x'$. Then, the balance of amplitudes is described by

$$\sqrt{\left(\omega \mathcal{Z}_x' \nu_y + \nu_x \omega \mathcal{Z}_y \right)^2 + \left(\omega^2 \mathcal{Z}_x \mathcal{Z}_y - \omega_c^2 - \nu_x' \nu_y \right)^2} = \frac{e \omega_c E_0}{m_e \omega s_{s,y}}. \tag{35}$$

In the limit of low ω and ν, this equation transforms into the usual Hall relationship $\omega s_{s,y} = cE_0/B$. The important point is that new functions $\mathcal{Z}_x'$ and ν_x' are much larger than $\mathcal{Z}_x$ and ν_x respectively because $\mathcal{N}_d$ and $\mathcal{M}_d$ contain the derivative $\partial/\partial a$ instead of $1/a$ entering $\mathcal{N}$ and $\mathcal{M}$, while the parameter $a = g_y s_{y,s}$ is very large due to a high Hall velocity (the first maximum of $\mathcal{N}$ occurs at $a \approx 50$).

A procedure similar to that used for obtaining Eq. (22) yields the following equation for the real part of magnetoconductivity

$$\sigma_{xx} = \frac{e^2 n_e}{m_e} \times$$

$$\times \frac{\nu_y(\omega_c^2 + \nu_x' \nu_y) + \nu_x \omega^2 \mathcal{Z}_y^2 + \nu_y \omega^2 \mathcal{Z}_y (\mathcal{Z}_x' - \mathcal{Z}_x)}{(\omega_c^2 + \nu_x' \nu_y - \omega^2 \mathcal{Z}_x \mathcal{Z}_y)^2 + \omega^2 (\mathcal{Z}_x' \nu_y + \mathcal{Z}_y \nu_x)^2}. \tag{36}$$

To include the contribution from direct scattering of electrons by thermally excited ripplons one should add ν_e to each ν_p and ν'_x. This equation differs substantially from the conventional Drude form. The usual magnetoconductivity equation follows from Eq. (36) if we consider the low frequency limit and assume that $\nu_y = \nu_x = \nu'_x$. As noted above, this simple approximation cannot be used here because $|\mathcal{Z}'_x| \gg |\mathcal{Z}_x|$ and $|\nu'_x| \gg |\nu_x|$ if $g_y s_{y,s} \gg 1$.

In the conventional magnetoconductivity treatment based on the Drude equation, there is a strict relationship between σ_{xx} and $\mu = e/m_e\nu$, and one can expect a certain accordance of magnetoconductivity data with mobility data. The appearance of new quantities $\mathcal{Z}'_x$ and ν'_x which differ greatly from $\mathcal{Z}$ and ν_D entering Eq. (22) means that such an accordance is impossible for the nonlinear WS transport over superfluid ^{4}He.

Typical dependencies of σ_{xx}^{-1} on the WS velocity $u = \omega s_{y,s}$ normalized to a ripplon velocity $u_R = \omega_{r,g_1}/g_1$ are shown in Fig. 9 for two electron densities. The conditions of the system were chosen to be very close to those of the experiment [5,6]. It is important that σ_{xx}^{-1} rapidly falls down before the Bragg-Cherenkov threshold, approaching a minimum which is below the experimental data. After the minimum the dependence $\sigma_{xx}^{-1}(u)$ is similar to the dependence $\sigma_{xx}^{-1}(V_{\rm in})$ observed in the experiment (assuming that u_y is approximately proportional to $V_{\rm in}$): $\sigma_{xx}^{-1}(u)$ increases, attains a maximum and starts falling down again. The new fall ends by sharp changes of $\sigma_{xx}^{-1}(u)$ leading to instability because σ_{xx} becomes negative when u exceeds a certain threshold value $u_{\rm th}$ which is larger than the Bragg-Cherenkov threshold. Before attaining negative values, $\sigma_{xx}^{-1}(u)$ demonstrates a vertical jump, which also agrees with experimental observations. The condition $\sigma_{xx} < 0$ means that any density fluctuation grows [21] and, therefore, the long-range order is expected to be destroyed. The threshold value $u_{\rm th}$ changes in a non-monotonous way even for very small variations of n_e, and in the interval $1\cdot10^8\,{\rm cm}^{-2} < n_e < 1.3\cdot10^8\,{\rm cm}^{-2}$ the ratio $u_{\rm th}/u_1$ can substantially exceed the values indicated in Fig. 9.

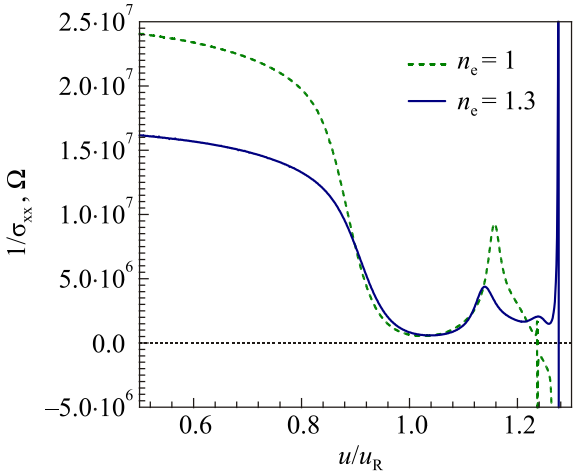

Fig. 9. (Color online) Inverse conductivity vs the WS velocity $u = \omega s_{y,s}$ normalized to $u_R = \omega_{r,g_1}/g_1$. Two electron densities n_e are shown in units of $10^8\,{\rm cm}^{-2}$. The damping parameter $\gamma' = 0.005$. Other conditions are the same as in the experiment [5,6].

6. Conclusions

In this work, we theoretically investigated the nonlinear responce of the liquid helium surface to an oscillating motion of the 2D Wigner solid on the surface of superfluid helium. The response force applied to the WS consists of two different terms representing the effective mass of surface dimples and the kinetic friction. The electron pressure acting on the free surface is a nonlinear function of the electron current which induces superharmonic resonances of the ripplon field and the response force. As a result, the dimple mass and the kinetic friction change sharply when the WS is driven with a frequency which is close to subharmonics of the frequency of a ripplon whose wave vector coincides with a reciprocal-lattice vector. In the limiting case of zero ripplon damping, the dimple mass and the effective collision frequency as functions of frequency have an infinite number of singular points. Therefore, any low driving frequency is close to a singular point, which means that WS transport over superfluid ^{4}He is singular and a small variation in the electron density can cause large changes (even qualitative) in nonlinear transport properties of the WS.

We found that our calculations of the nonlinear WS mobility and the dimensionless mass function are in good qualitative accordance with experimental observations [8,20] which previously had no theoretical explanations. The analysis of nonlinear phonon-ripplon coupling given in this work explain observation of new low-frequency resonances [8] and the strange behavior of conventional phonon-ripplon coupled modes with an increase of the excitation signal.

Considering magnetotransport of the 2D WS in an oscillating electric field, we found that the nonlinear magnetoconductivity tensor cannot be reduced to the conventional Drude form, and, therefore, an accordance between nonlinear mobility and magnetoconductivity data is impossible. In the direction of the driving electric field, the dimple mass and effective collision frequency acquire huge values exceeding greatly those of the mobility treatment. Moreover, at a sufficiently high electron velocity in the perpendicular direction, the magnetoconductivity becomes negative which causes instability and fluctuational melting of the WS. The dependence of nonlinear magnetoconductivity on the velocity amplitude obtained in this work can be used also as an alternative explanation of the remarkable dynamic transition observed long ago [5,6].

1. C.C. Grimes and G. Adams, *Phys. Rev. Lett.* **42**, 795 (1979).
2. Yu.P. Monarkha and V.B. Shikin, *Zh. Eksp. Teor. Fiz.* **68**, 1423 (1975) [*Sov. Phys. JETP* **41**, 710 (1975)].

3. D.S. Fisher, B.I. Halperin, and P.M. Platzman, *Phys. Rev. Lett.* **42**, 798 (1979).
4. R. Giannetta and L. Wilen, *Solid State Commun.* **78**, 199 (1991).
5. K. Shirahama and K. Kono, *Phys. Rev. Lett.* **74**, 781 (1995).
6. K. Shirahama and K. Kono, *J. Low Temp. Phys.* **104**, 237 (1996).
7. A. Kristensen, K. Djerfi, P. Fozooni, M.J. Lea, P.J. Richardson, A. Santrich-Badal, A. Blackburn, and R.W. van der Heijden, *Phys. Rev. Lett.* **77**, 1350 (1996).
8. V. Sivokon', V. Dotsenko, Yu. Kovdrya, and V. Grigor'ev, *J. Low Temp. Phys.* **111**, 609 (1998).
9. Yu.P. Monarkha, *Europhys. Lett.* **118**, 67001 (2017).
10. K. Shirahama, O.I. Kirichek, and K. Kono, *Phys. Rev. Lett.* **79**, 4218 (1997).
11. Yu.P. Monarkha, and K. Kono, *J. Phys. Soc. Jpn.* **66**, 3901 (1997).
12. K. Shirahama, Yu. P. Monarkha, and K. Kono, *Phys. Rev. Lett.* **93**, 176805 (2004).
13. P. Roche, M. Roger, and F.I.B. Williams, *Phys. Rev. B* **53**, 2225 (1996).
14. Yu.P. Monarkha and K. Kono, *Two-Dimensional Coulomb Liquids and Solids* Springer-Verlag, Berlin (2004).
15. Yu. P. Monarkha and K. Kono, *J. Phys. Soc. Jpn.* **75**, 044601 (2006).
16. P. Glasson, V. Dotsenko, P. Fozooni, M.J. Lea, W. Bailey, and G. Papageorgiou, *Phys. Rev. Lett.* **87**, 176802 (2001).
17. Yu.P. Monarkha and K. Kono, *Fiz. Nizk. Temp.* **35**, 459 (2009) [*Low Temp. Phys.* **35**, 356 (2009)].
18. M.I. Dykman and Yu.G. Rubo, *Phys. Rev. Lett.* **78**, 4813 (1997).
19. Yu.P. Monarkha and K. Kono, *J. Phys. Soc. Jpn.* **70**, 1617 (2001).
20. V.E. Syvokon and K.A. Nasedkin, *Fiz. Niz. Temp*. **36**, 1267 (2010) [*Low Temp. Phys.* **36**, 1023 (2009)].
21. Yu.P. Monarkha, *Fiz. Nizk. Temp*. **42**, 657 (2016) [*Low Temp. Phys.* **42**, 441 (2016)].